Fast scanning probe for tokamak plasmas

J. Boedo, D. Gray, L. Chousal, and R. Conn
Department of Applied Mechanics and Engineering Sciences, University of California, San Diego, Mail Code 0417, 9500 Gilman Drive, La Jolla, California 92093

B. Hiller and K. H. Finken
Institut für Plasmaphysik, Forschungszentrum Jülich GmbH, Postfach 1913, 52425 Jülich, Germany

(Received 11 April 1997; accepted for publication 31 March 1998)

We describe a fast reciprocating probe drive, which has three main new features: (1) a detachable and modular probe head for easy maintenance, (2) a combination of high heat flux capability, high bandwidth, and low-Z materials construction, and (3) low weight, compact, inexpensive construction. The probe is mounted in a fast pneumatic drive in order to reach plasma regions of interest and remain inserted long enough to obtain good statistics while minimizing the heat flux to the tips and head. The drive is pneumatic and has been designed to be compact and reliable to comply with space and maintenance requirements of tokamaks. The probe described here has five tips which obtain a full spectrum of plasma parameters: electron temperature profile $T_e(r)$, electron density profile $n_e(r)$, floating potential profile $V_f(r)$, poloidal electric field profile $E_\theta(r)$, saturation current profile $I_{\mathrm{sat}}(r)$, and their fluctuations up to 3 MHz. We describe the probe show radial profiles of various parameters. We compare the density and temperature data to that obtained with a helium beam. We also discuss the techniques to process the data optimally, particularly double probe data and profile fits. © *1998 American Institute of Physics.* [S0034-6748(98)00307-4]

I. INTRODUCTION

Characterizing the plasma edge and scrape-off layer (SOL) of fusion devices is important to gage discharge performance, understand the properties of the edge and SOL plasmas,[1] evaluate their interaction with the plasma facing components,[2] and to understand some of the basic physics issues such as turbulence and anomalous radial particle transport.[3] Understanding the tokamak boundary has profound implications for large fusion projects such as the International Thermonuclear Experimental Reactor (ITER) and future fusion devices since their performance is limited by the heat load on the plasma facing wall. The future fusion needs are therefore driving an effort in plasma modeling,[4,5] which requires a large database for validation and scaling purposes.

In recent years, a growing awareness that the plasma edge is determinant for the establishment of high confinement regimes (H mode, VH mode, etc.),[6–9] is driving a significant amount of research and diagnostic development for the edge, since it is generally believed that the origin of anomalous edge particle transport in tokamaks is electrostatic turbulence-driven transport,[8–11] which can be fully evaluated only with probes. With some of these needs in mind, we have developed the probe described here.

Scanning probes have been utilized very successfully in the past to diagnose plasmas in small plasma experiments and the semiconductor-processing industry but those plasmas are considerably colder and less dense than those present in fusion devices so the development of probes for fusion has been driven by a different set of challenges. Original fast scanning probe designs[3,12] were all metal construction and therefore not suitable for today's high performance machines, where the high plasma temperature and density would erode the metal tips and contaminate the plasma with high Z materials. New probe systems have been developed recently for the newer, high-performance fusion devices, and are designed specifically[2,13] to reduce plasma contamination, resist high heat and particle flux, and withstand forces induced by disruptions. The new probes tend to be very complex, large, heavy, and expensive, and it would be desirable to address some of these issues in a new design.

In this article we describe a probe that features some improvements such as a modular head and tip design for ease of replacement, compactness, simplified reciprocating action, low-Z materials head construction, high bandwidth operation to 3 MHz for turbulence measurements, high speed operation, and high heat flux capability. In short, we have incorporated many of the best features of existing designs and alleviated some of their shortcomings. We will devote this article to the description of these features, how they have been achieved, and how they meet the stringent requirements imposed by the Torus Experiment for Technology Oriented Research (TEXTOR) plasmas.

II. PROBE DESCRIPTION

We have incorporated a variety of characteristic features in the design of the probe; among them are: the modular design of the probe head, the use of lightweight materials in the probe head and feedthrough, a compact two-stage drive design, and the extensive use of off-the-shelf components in combination with an all-coaxial design for high bandwidth operation. We describe these features in detail in the subsequent sections.

The probe assembly consists of two main parts: the drive mechanism and the probe itself, both mounted on an aluminum backbone which rests on an insulating table which con-

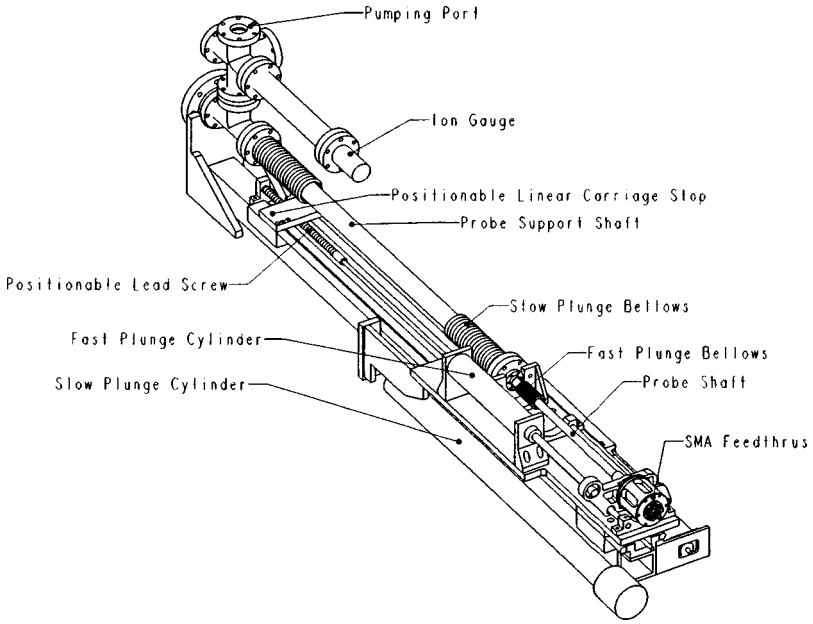

FIG. 1. Fast scanning probe view from the left showing the cylinders for the fast and slow plunges.

tains all the mechanisms, therefore making the instrument very portable. The probe interfaces to the tokamak through a front flange which is $\frac{1}{2}$ in. with a bore I.D. of $2\frac{1}{2}$ in. and is differentially pumped at 50*l*/s, the pressure being monitored with an ion gauge. A general view of the probe can be seen in Fig. 1.

A. Design requirements

The main criteria for the probe design are:
(i) Ability to obtain the needed measurements.

(1) Electron temperature $T_e(r)$ and density $n_e(r)$ profiles with 1–2 mm spatial resolution (less than the 6 mm profile decay length).
(2) Floating potential $V_f(r)$ and poloidal electric field $E_\theta(r)$ profiles with 2 mm spatial resolution.
(3) Profiles of fluctuation levels in density $\tilde{n}_e$, poloidal electric field $\tilde{E}_\theta$, plasma potential $\tilde{V}_p$, and electron temperature $\tilde{T}_e$ with a bandwidth of up to 3 MHz (we customarily operate up to 1 MHz) and spatial resolution of 2 mm.

(ii) Survive the plasma conditions. The probe shaft, head and tips should:

(1) withstand a heat flux of 10 MW/cm^2 while keeping the graphite head and tips temperature below 1600 °C;
(2) be compatible with a base pressure of 1×10^{-7} Torr;
(3) bebakeable to 150–200 °C;
(4) hold a potential of 3 kV to ground;
(5) be made of low Z materials so as not to contaminate the plasma;
(6) withstand forces generated by accelerations of up to 15 g.

(iii) Ease of maintenance and simplicity of operation.

(1) Due to the harsh conditions to which the probe is exposed, progressive damage to the tips and head occurs during normal use, a system to ease the replacement of those is mandatory in these probes.
(2) Access to diagnostics in tokamaks is usually impaired during operation due to neutron activation and space and time constrains. The reciprocating system should therefore be as reliable and simple as possible in order to reduce downtime and ease repairs.

B. Probe

The probe assembly is comprised of two main parts: the probe itself and the drive mechanism. The probe is composed of the head, shaft, and feedthrough and should be as light as possible in order to increase speed and decrease the forces generated during operation. The head is exposed to the harsh plasma conditions for a brief time and should be easily replaced or maintained.

1. Probe head

Five tips are required for our measurements, they are made out of POCO graphite and mounted on a boron nitride (BN) matrix for electrical insulation. The whole structure is protected against high heat fluxes by a graphite shroud, yet a small section of BN is exposed as shown on Fig. 2 (detail) in order to prevent the graphite (a conductor) from setting boundary conditions for the electric fields. The exposed dimensions of the tips are 1.5 mm length (l) and 1.5 mm diameter (d). The tips are filed to a tolerance of 0.1 mm in length by using a filing jig.

The probe tips are aligned as seen in Fig. 3 in such a manner that magnetic field angles between 0° and 13° are possible without mutual shadowing yet allowing them to sample approximately the same plasma. The standard TEXTOR magnetic field pitch angle is approximately 4° at the edge. Two tips (1,2) are used as a double probe pair, one tip is at ion saturation (5) and two poloidally separated tips (3,4)

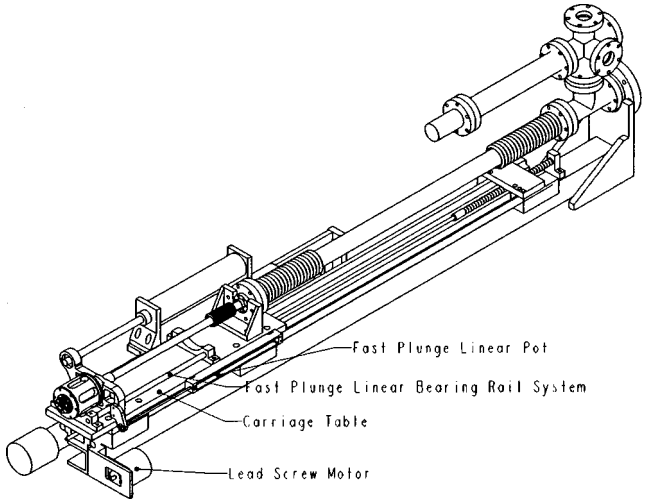

FIG. 2. Fast scanning probe view from the right showing the carriage table and the two sets of bellows.

are floating to measure the floating potential (and thereby, by substraction, the poloidal electric field). Tips 3 and 4 are made to float by attaching to each of them to a 100 kΩ vacuum resistor (much higher than the plasma sheath impedance). The tip assembly is then attached to coaxial cables.

The constant wear on the head and tips make it mandatory to periodically replace the tips and occasionally, the BN insulator and graphite shield. Exposure to carbon released from other plasma-facing components coats the BN insulating piece and therefore shorts the tips electrically (after a period of operation which depends on the plasma conditions). Given the limitations stated above, the head has been designed in such a way that parts replacement is a fast and simple operation.

The approach taken in our design is shown in Fig. 2 and it consists of three removable BN sections. The first one is fixed to the shaft and features pin connectors, the second one is a buffer piece which holds the connections to the tips (resistors or matching wires depending on the tip), and the third holds the tips in place and is partially exposed to the plasma. All the BN pieces are notched as shown in Fig. 4 in order to prevent rotation during assembly and operation. The tips are threaded in the back to accept a short piece of oxygen-free copper wire, the other end of the wire has Inconel sockets crimped to it which mate to the pins in the support section. The head assembly is held in place by the graphite shield screwed onto the Inconel shaft at 11 threads/cm. The inside bore of the graphite shield and the outside shape of the BN holder (Fig. 2 detail) are conical to prevent releasing the head into the plasma in case of breakage and assure better distribution of the forces during the probe plunge (increasing the contact area).

2. Shaft

The probe shaft is made out of Inconel tubing, 1.25 cm in diameter which features the head assembly at the front end and houses a set of semirigid coaxial vacuum cables within a thin ceramic tube which provides electrical isolation. The coaxial cables act as transmission lines (50 Ω load), assuring good frequency response. The cables connect the tip assembly to a SMA-based feedthrough system which is fastened to the probe shaft and to an aluminum base mounted on a linear bearing system, as show in Figs. 1 and 4. In order to reduce weight, the feedthrough system is custom designed and built out of polyimide (Vespel trademark by Dupont). This material is easy to machine, lightweight, and strong (85-95 Rockwell *H*), resist high temperatures (300 °C), and has a very low outgassing rate[14] (4×10^{-10} Torr ℓ/s cm^2 at room temperature and 3×10^{-6} at 300 °C). Vespel is slightly higroscopic and absorbs water upon air exposure which is then released during bakeout; therefore Vespel is used only on the back of the probe shaft, which is at room temperature.

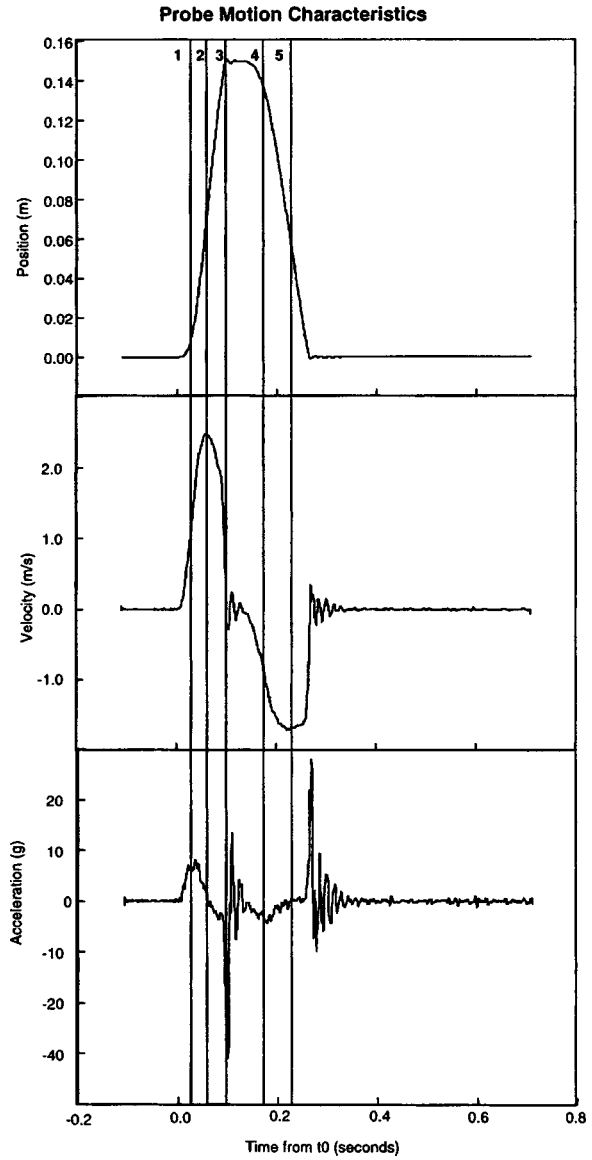

FIG. 3. The upper panel shows the probe position, the middle one the velocity, and the lower one the acceleration of the probe. Times of interest are marked; for the inward plunge, time 1 is when the maximum acceleration occurs, time 2 is when the maximum velocity is achieved, time 3 is when the maximum decceleration happens and the beginning of the dwell time, and times 4 and 5 are the equivalent for the outward plunge.

C. Probe drive

The probe drive mechanism should be made as fast as possible in order to limit the time of exposure of the probe

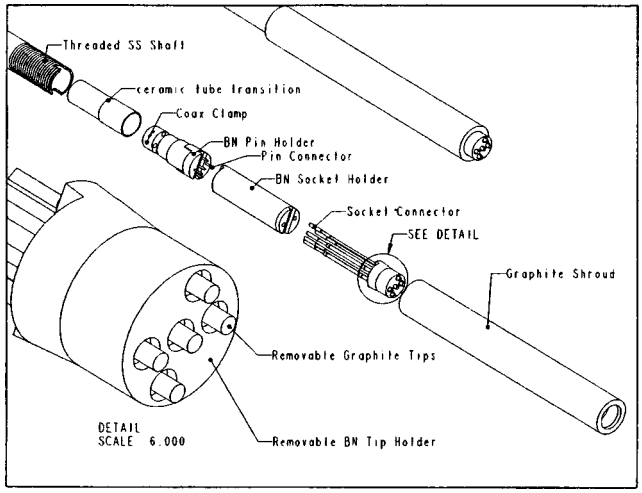

FIG. 4. Probe head assembly and detail of BN tip holder showing the modular construction which allows fast tip replacement.

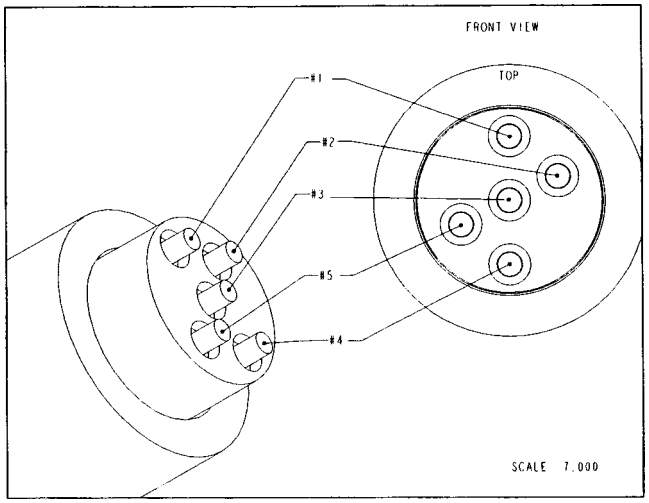

FIG. 5. Probe tip geometry and detail. Tips 1 and 2 are a double probe, tips 3 and 4 measure the floating potential, and tip 5 measures I_{sat}. The parallel magnetic field B_ϕ is sloping gently (4°) horizontally from left to right.

head and tips. The probe drive design is therefore a compromise between the desire to obtain enough statistics on the data and reducing damage to the probe at a reasonable cost. We have developed a distinctive, compact two-stage design drive using as many off-the-shelf parts as possible to reduce costs.

The drive mechanism is a two-stage pneumatic system based on the philosophy that the probe should move powered by a slow pneumatic cylinder to a stand-by position where it is not exposed to the plasma and then should reciprocate from there rapidly, powered by a fast cylinder when triggered by the control system. Therefore, the probe assembly consists of a fast plunge section which is carried on top of a slow plunge section. The pneumatic drive is rugged and dependable and, we find, very accurate with position reproducibility to within 5%.

The slow plunge section consists of a carriage table which is fastened to bearing sliders (Thomson DSRC-8) as shown in Figs. 1 and 4 which moves on a linear track (Thomson DSRA-8) fastened to the probe backbone. This section is moved by an Allenair SVS-E-AA pneumatic cylinder 1.5 in. in diameter with a 18 in. stroke and powered by 5 bars of compressed air. The fast moving section (fast cylinder, shaft, and fast plunge bellows) is mounted on the carriage table. An inherent advantage of this setup is that in the case of a vacuum accident, a relatively fast retrieval of the probe (1 s) behind a gate valve by the slow pneumatic cylinder is possible. The position where the carriage stops is adjustable and determined by a stop-block that can be moved by a step motor-activated lead screw. The stop position can be varied by 12 cm and determines the deepest penetration of the probe. The slow plunge cylinder is located along the backbone and under the carriage table as seen in Fig. 1, thereby reducing the probe assembly length and weight; this is a distinctive feature of our design which helps to make the probe more compact and a clear improvement over previous designs.[2,3]

Once the slow plunge section is placed in position the fast plunge section, moved by an Allenair A-BC-RR-L cylinder powered by helium at 4 bars, reciprocates when the fast valve is triggered by the control system. This type of cylinder does not offer a readily variable dwell penetration or detailed timing for the probe since its operation is ''programmed'' initially by the settings of the mechanical exhaust valves, but it does offer improvements in operation simplicity, maintenance, and excellent performance. The length of the fast stroke is fixed to 6 in. (15 cm). This feature is also distinctive of our design and trades the flexibility of a fully programmable stroke for simplicity and lower weight.

The position of the probe as a function of time is digitized from a potentiometer at 40 kHz and shown in Fig. 5 together with the velocity and acceleration. The times of interest are labeled from 1 to 5. The speed and acceleration are shown in Figs. 5(b) and 5(c), respectively. At time 1, shortly after the beginning of the plunge, the acceleration is at a maximum (8 g), causing the probe to reach its maximum speed of 2.5 m/s at time 2. Briefly thereafter, the deceleration starts to bring the probe to a halt (time 3). At this time, there is a transient acceleration of about 10 g and the probe starts moving back at a considerably lower acceleration due to a drop in helium pressure in the lines and reservoir. It is important to mention that the substantially higher speed of sound in helium offers improved performance over air and that the use of a gas reservoir to maintain the helium pressure during operation is crucial.

III. MEASUREMENTS IN TEXTOR

The probe is located in the outer midplane of the machine, where the toroidal magnetic field B_T is roughly 18 kG during standard operation and therefore the size of the ion and electron gyroradius are $\rho_e \approx 1\times10^{-3}$ cm, $\rho_i \approx 2-8\times10^{-2}$ cm for the range of electron (T_e) and ion (T_i) temperatures encountered in the TEXTOR edge ($T_i \approx 10-250$ eV, $T_e \approx 10-130$ eV) which means we operate in the very strong magnetic field regime and the probe dimensions are much larger than the ion ρ_i and electron ρ_e gyro-

radius $d=0.15\ \text{cm} > \rho_i(0.2\ \text{mm}) \gg \rho_e(0.01\ \text{mm})$[1] and should use the projected area A_p of the probe tips as the collection area[15] i.e., $A_c=A_p=2\times l\times d$ or 4.5 mm^2.

The probe tips, of length l and diameter d, collect plasma from—and therefore average over—a certain length along the magnetic field called collection tube. The toroidal extent L_p of this perturbation can be estimated[1] if we know the ion perpendicular diffusion coefficient $D_\perp$ and the sound speed c_s by:

$$L_p \approx (d\times l\times c_s)/(8\times D_\perp). \tag{1}$$

For the values of T_e and T_i given above and using $D_\perp = 0.6-1\ \text{m}^2/\text{s}$[1,16] we obtain $L_p \approx 28$ mm. Therefore the data are averaged over 2.8 cm in the toroidal direction, averaging that does not affect our results since the parallel gradients in most tokamaks are only appreciable in the vicinity of significant sinks or sources of particles and energy such as those present near limiter and divertor plates.

The probe measures radial profiles of the floating potential $V_f(t)$ at two poloidal locations; thereby we can calculate the poloidal electric field $[E_\theta(t)]$ and the radial electric field E_r. The saturation current $I_{\text{sat}}(t)$, and continuous double probe characteristics are obtained as well. The maximum error we expect from a high radial field (highest measured $E_r = 450$ V/cm) showing as E_θ due to tip length differences is 4 V; under normal conditions, the error is less than 0.5 V. We measure fluctuations at a digitization rate of 1–2 MHz although the probe system has been designed for and complies with a bandwidth of 3 MHz. The double probe is swept with a 400–700 Hz sawtooth voltage of amplitude $+-200$ V as shown in Fig. 6 in order to provide a full current–voltage $(I-V)$ characteristic every 3 ms. This provides values of the plasma electron density n_e and temperature T_e by fitting the function:

$$I = I_{\text{sat}}\times \tanh(eV_a/2k_bT_e). \tag{2}$$

Here $I_{\text{sat}} = 0.5\times A_p \times e \times n_e \sqrt{k_b\times(T_e+T_i)/m_i}$ where we usually assume $T_i \approx T_e$ (which is *not* true in general in the edge plasma in TEXTOR,[17] but is a good operating assumption since the current is a weak function of the temperature) and V_a is the difference between the probe and the floating potentials. The fit is done with four variables because offsets in the voltage and current are allowed, but convergence is usually straightforward. The signal to noise ratio (S/N) limit varies depending on plasma conditions, but reliable profiles are obtained up to 3–4 cm into the SOL, where the low I_{sat} causes loss of sensitivity on the variation of T_e. Our codes provide options for averaging 2 or 3 sweeps in order to improve the S/N ratio in exchange for some loss in spatial resolution. We thereby produce values of n_e and T_e as a function of time as shown in Fig. 7. Since the applied voltage must be on the order of $2\times kT_e$ to assure current saturation and our power supply is limited to 200 V, our temperature limit is about 100 eV, but we find that we can get reliable temperatures up to 120 eV since we fit a known, very nonlinear function and therefore the routine is able to calculate an I_{sat} compatible with the partial data. These signals are digitized at 40 kHz to resolve enough points (between 120 and 300) per sweep. It is interesting to note that the error of the fitting varies with the sweep rate. This is due to the fact that large density fluctuations (on the order of 40%) exist at the plasma edge and the spectrum of these fluctuations peaks at fairly low frequencies (0–50 kHz). It can, therefore be deleterious to sweep too fast since the fluctuations are not integrated over time and the data are more noisy. We have found that a good compromise between good spatial (temporal) resolution and better fits exists at about 600 Hz.

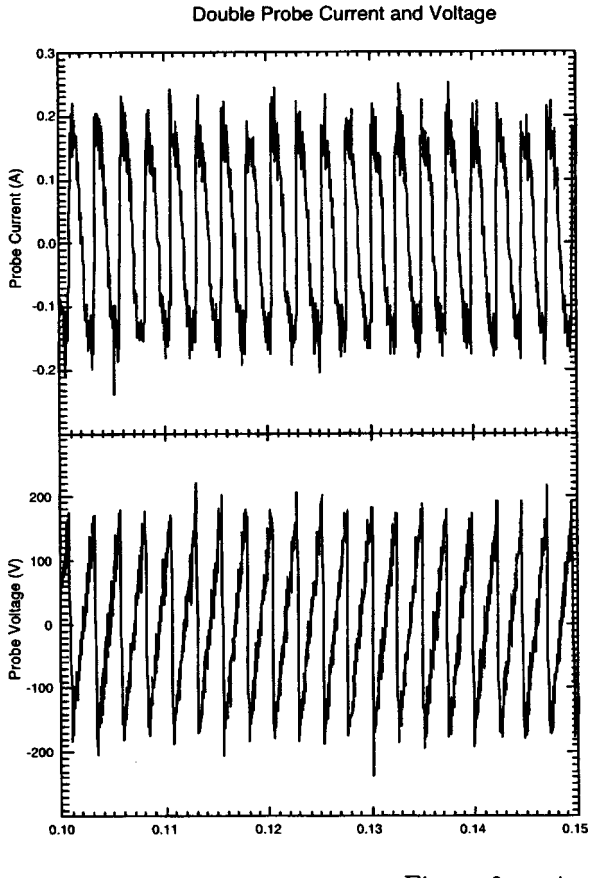

FIG. 6. Traces showing double probe voltage (lower panel) and current (upper panel). This signals are measured near the plasma and at high bandwidth and show plasma fluctuations.

The double probe has the advantage that it is insensitive to high local voltages as found in the case of limiter biasing[18] or edge polarization[19] since it is a floating system. The tip that measures I_{sat} is, on the other hand, a single probe and biased by a power supply referenced to limiter ground and therefore is liable to lose saturation if the plasma potential is highly negative. To avoid this problem, we reference the I_{sat} power supply to the shaft of the probe, which is floating at a potential usually dominated by the plasma with the highest temperature and density or the highest floating potential (if externally applied). The area of the probe shaft exposed to the plasma is roughly 40 cm^2. We have satisfactorily compared the I_{sat} signal with the envelope of the double probe current sweeps.

The radial profiles of all the quantities of interest can be reconstructed from the time–position information. The spatial resolution will depend on the voltage sweep frequency (400–700 Hz) and the velocity of the probe, which is vari-

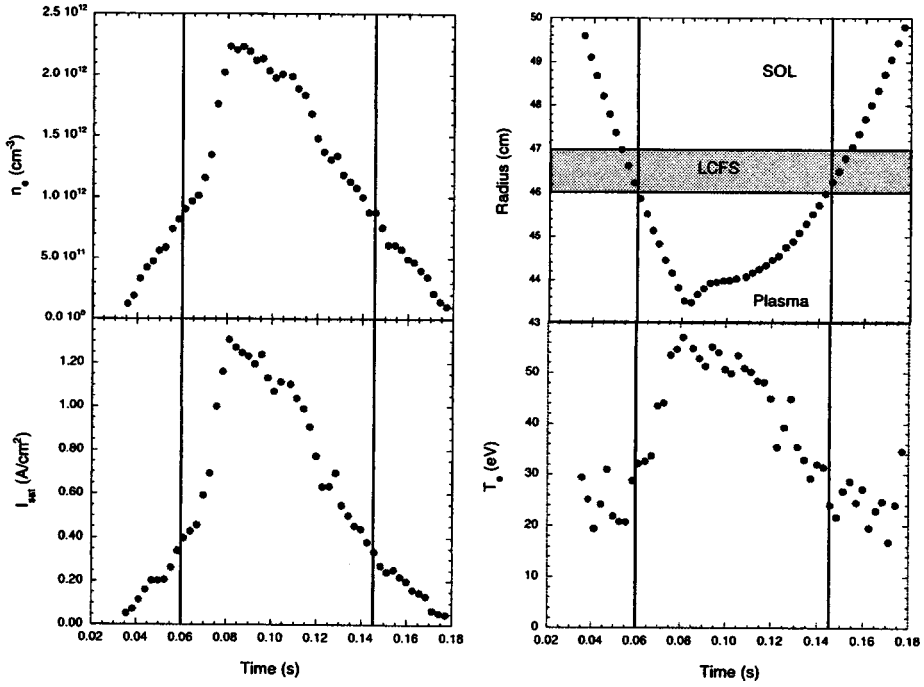

FIG. 7. Probe traces of: upper right, probe position, lower right, electron temperature, upper right, density and lower right, saturation current for a low density OH TEXTOR discharge. The ALT-II limiter is marked as a shaded square and the times when the probe crosses the LCFS are marked with vertical lines. The probe penetrates about 2.5 cm in the plasma.

able with radius. At its fastest (2.5 m/s), the probe moves about 2–6 mm during a double probe sweep, that is in 1–3 ms, therefore the spatial resolution of the double probe measurements varies from 1 to 2 mm (order of tip length) to 6 mm (four tip lengths). Typical spatial resolution in the plasma is 1–2 mm because the probe moves slowly only outside the plasma as seen in Fig. 7. Typical profiles of the electron density and temperature for a high power discharge are shown in Fig. 8.

We have compared the profiles of T_e and n_e with those obtained from a helium beam[20,21] for two high performance RIM-mode[22] TEXTOR discharges. One of the discharges (67135) features high radiated fraction. We found excellent agreement (within 15%) for the densities in the range 46.5–50 cm as shown in Fig. 9 and the difference between the two diagnostics becomes noticeable at 46.5 cm due to fact that the beam attenuates rapidly with penetration and therefore uncertainty as explained by Schweer.[20,21] The temperature profiles are compared in Fig. 10 and agreement within 15% is found up to $r=47$ cm, from there up to $r=48.5$ agreement exists within 30%. The probe has a larger penetration than the beam (which is limited at high densities) and has the intrinsic advantage that the data can be easily processed in real time since it does not involve any atomic models.

There is a marked advantage of probes over atomic beams on the evaluation of density and temperature values at the last closed flux surface (LCFS) and SOL decay lengths; the beams rely on a radial calibration that is sensitive to changes in plasma position and therefore a small error in position will translate into large differences on the values calculated due to the exponential behavior of the profiles. The position of the LCFS has as its signature a sudden drop

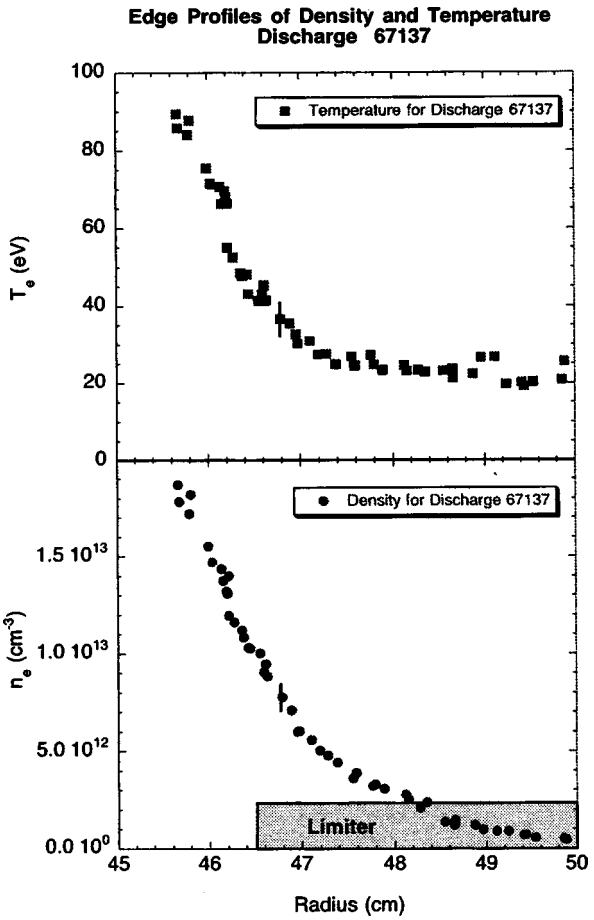

FIG. 8. Radial profiles of electron temperature and density for a high power TEXTOR discharge.

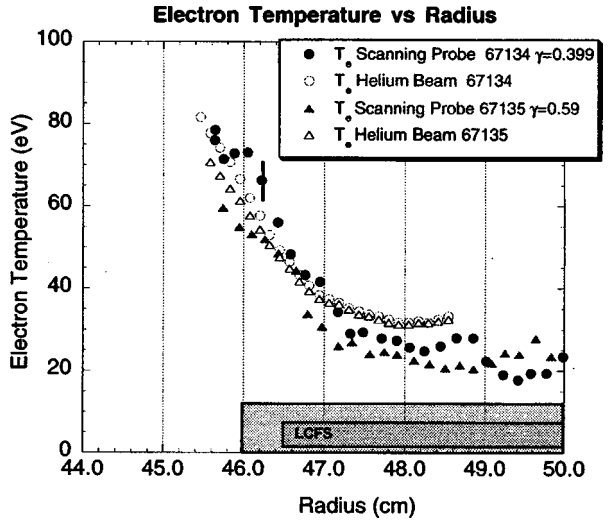

FIG. 9. Traces of electron density from the probe (filled symbols) and a helium beam (open symbols) for a high performance RIM-mode TEXTOR discharge. The position of the LCFS is as in the previous figure.

in the floating potential profile which can be detected easily by probes with an accuracy of 1–2 mm and therefore it provides a self-calibrating positioning for the LCFS.

The probe can also provide simultaneous measurements of the fluctuating quantities $\tilde{E}_\theta$ and $\tilde{n}_e$ and from them infer turbulent particle and heat transport as described by Liewer[23] and Powers.[24] These measurements are necessary in order to understand the underlying cause of anomalous energy losses in tokamaks and characterizing them and, at the moment, can be performed only by probes. The turbulence-induced flux $\tilde{\Gamma}$ can be written in terms of an ensemble average of the density fluctuation level $\tilde{n}_e$ and the velocity fluctuation level $\tilde{V}$ (in the direction of the flux) as:

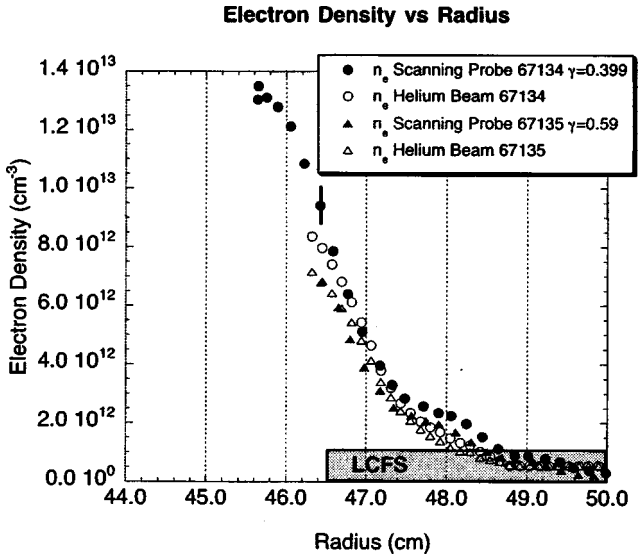

FIG. 10. Traces of electron temperature from the probe (filled symbols) and a helium beam (open symbols) for two high performance RIM-mode TEXTOR discharges (67134 and 67135) The radiated power fraction γ is varied by almost a factor of 2 by injecting neon in the discharge. The nominal position of the nominal ALT-II limiter radius is marked as a shaded square, but the LCFS is actually found slightly more outward as noted due to plasma shifts, the probe penetrates about 10 mm in the plasma.

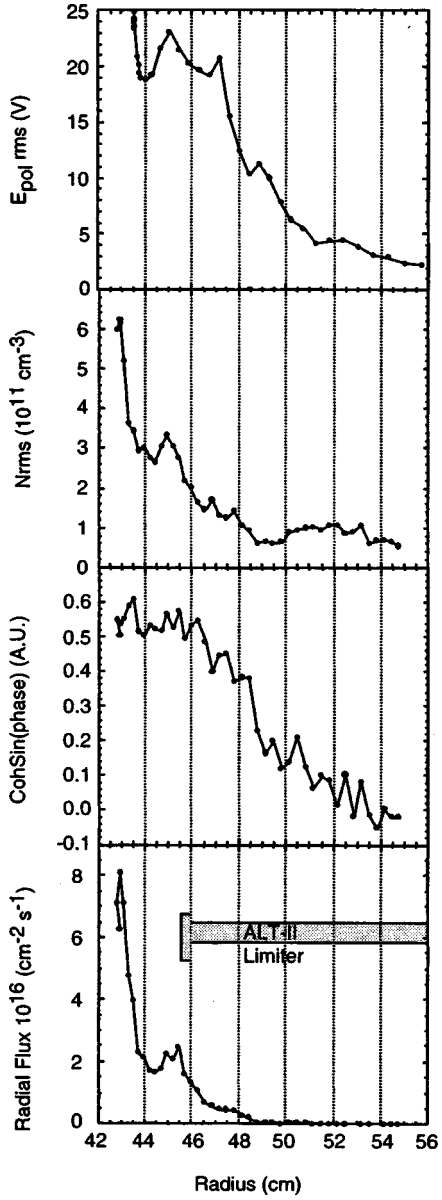

FIG. 11. Traces of (from top to bottom): $\tilde{E}_\theta$, $\tilde{n}_e$ rms, cos $\alpha_{\tilde{n}_e\tilde{E}_\theta}$, and $\tilde{\Gamma}_r$ for a low current and density TEXTOR discharge. The ALT-II limiter is marked as a shaded square.

$$\tilde{\Gamma}=\langle\tilde{n}\tilde{V}\rangle. \tag{3}$$

With the assumption $|k|\rho_i<1$ the expression for the radial flux becomes:

$$\tilde{\Gamma}_r=\langle\tilde{n}\tilde{V}_r\rangle=\left\langle\frac{\tilde{n}_e\tilde{B}_\theta}{|B_\phi|}\right\rangle=\frac{\langle\tilde{n}_e^2\rangle^{1/2}\langle\tilde{E}_\theta^2\rangle^{1/2}}{B_\phi}\frac{\langle\tilde{n}_e\tilde{E}_\theta\rangle}{\langle\tilde{n}_e^2\rangle^{1/2}\langle\tilde{E}_\theta^2\rangle^{1/2}} \tag{4}$$

TABLE I. A summary of the main edge and SOL parameters for Ohmic discharges in TEXTOR are shown.

	$\left(\frac{\tilde{n}}{n}\right)_{SOL}$	$\left(\frac{\tilde{T}}{T}\right)_{SOL}$	$\left(\frac{\tilde{V}_f}{kT}\right)_{SOL}$	$\left(\frac{\tilde{n}}{n}\right)_{edg}$	$\left(\frac{\tilde{T}}{T}\right)_{edg}$	$\left(\frac{\tilde{V}_f}{kT}\right)_{edg}$
TEXT	0.3–0.5	0.15–0.2	0.2–0.5	0.2	0.1	0.3–0.5
TJ-1	⋯	⋯	⋯	0.3–0.5	0.4–0.5	⋯
DIII-D	0.2–0.5	N/A	0.3–0.6	0.1–0.2	N/A	0.1–0.3
TEXTOR	0.2–0.3	0.2–0.7	0.3–0.7	0.15–0.25	0.2	0.2–0.4

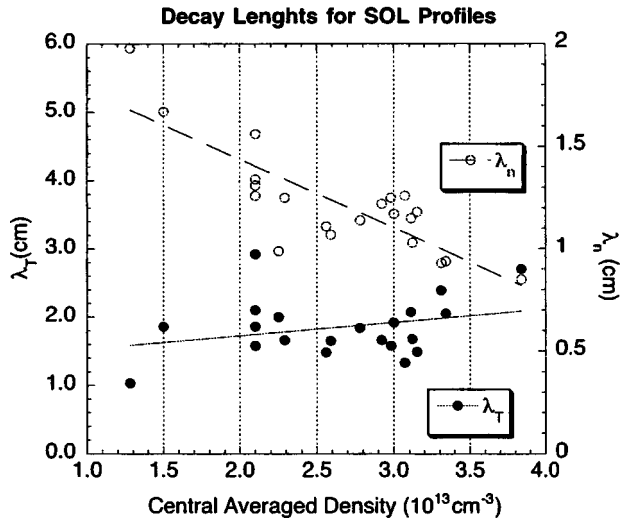

FIG. 12. Density (open circles) and temperature (solid circles) decay lengths in the SOL of TEXTOR for ohmic discharges. The plots include a wide variety of ohmic discharges. The dependence of λ_T with average central density is weak.

so it can be written in terms of the phase angle as:

$$\tilde{\Gamma}_r = \frac{\langle \tilde{n}_e^2 \rangle^{1/2} \langle \tilde{E}_\theta^2 \rangle^{1/2}}{B_\phi} \times \cos\, \alpha_{\tilde{n}_e \tilde{E}_\theta}. \tag{5}$$

Plots of the turbulence-driven particle flux $\tilde{\Gamma}_r$, the rms levels of n_e, E_θ, the cosine of the phase angle between them $\cos\, \alpha_{\tilde{n}_e \tilde{E}_\theta}$ are show in Fig. 11 for an ohmically heated (OH) discharge (69135). We have obtained such quantities for a large variety of TEXTOR discharges and summary of the results and a comparison to other tokamaks for OH conditions is shown in Table I.

Profiles of T_e and n_e are needed as input for codes which model the edge and SOL[5] of tokamak plasmas by solving a set of coupled nonlinear fluid equations and a neutral source. The calculations of these codes are needed for a deeper understanding of edge plasma issues and their implications for heat and particle exhaust in future fusion reactors. The data are also needed to evaluate the plasma interaction with the walls and to produce scalings which will help in the understanding and design of future machines. We find that the profiles in the SOL of TEXTOR are best fitted by the functions:

$$n_e(r) = n_{e0} + n_e(a) \times \exp[-(r-a)/\lambda_n], \tag{6}$$

$$T_e(r) = T_{e0} + T_e(a) \times \exp[-(r-a)/\lambda_T], \tag{7}$$

where a is the radius of the last closed flux surface (or limiter radius), n_{e0} and T_{e0} are offsets, and λ_n, λ_T are the characteristic decay length. It is crucial to notice that there is an offset on both the density and temperature profiles which will make purely exponential profile fits yield the wrong decay lengths. Exponential profiles are expected for simple, sourceless SOL, so the physical origin of the offset is probably the fact that the SOL has a significant particle source in it due to several reasons, photoionization, charge exchange of fast ions, and large banana orbit ions. A summary of the electron temperature and density LCFS decay lengths for OH conditions is shown in Fig. 12 against central-averaged density; notice that the temperature decay length is lightly dependent on average density but the density decay length is inversely dependent.

ACKNOWLEDGMENTS

This work has been supported by DOE Contract No. DE-FG03-85 ER 51069. Thanks are due to Dr. C. Castro for his inspirational influence to think greater things, and to Dr. J. Rapp and S. Jachmich for their friendship, and to R. Moyer for providing excellent feedback.

[1] P. C. Stangeby and G. M. McCracken, Nucl. Fusion **30**, 1225 (1990).
[2] J. G. Watkins *et al.*, Rev. Sci. Instrum. **3**, 4728 (1992).
[3] T. L. Rhodes, C. P. Ritz, R. D. Bengtson, and K. R. Carter, Rev. Sci. Instrum. **61**, 3001 (1990).
[4] M. Baelmans, PhD thesis, Katholieke Universiteit Leuven, 1994, KFA Tech. Rep. Jül-2891.
[5] M. Baelmans, D. Reiter, R. R. Weynants, and R. Schneider, J. Nucl. Mater. **1**, 466 (1992).
[6] K. Itoh, S.-I. Itoh, M. Yagi, and A. Fukuyama, Plasma Phys. Controlled Fusion **1**, 66666 (1996).
[7] Ch. P. Ritz, H. Lin, T. L. Rhodes, and A. J. Wooton, Phys. Rev. Lett. **65**, 2543 (1990).
[8] T. L. Rhodes, C. P. Ritz, and R. D. Bengtson, Nucl. Fusion **33**, 1147 (1993).
[9] R. Moyer *et al.*, Phys. Plasmas **2**, 2397 (1995).
[10] W. Rowan *et al.*, Nucl. Fusion **2**, 1105 (1987).
[11] G. R. Tynan *et al.*, Phys. Plasmas **1**, 3301 (1994).
[12] Ch. P. Ritz, H. Y. Tsui, T. L. Rhodes, Roger D. Bengtson, H. Lin, and A. J. Wooton, Rev. Sci. Instrum. **61**, 2998 (1990).
[13] J. G. Watkins *et al.*, Rev. Sci. Instrum. **68**, 373 (1997).
[14] P. W. Hait *et al.*, in 13th Vacuum Symposium of the American Vacuum Society, 1996, Vol. 1, p. 678.
[15] R. Pitts *et al.*, Nucl. Fusion **30**, 789 (1990).
[16] D. S. Gray *et al.*, Nucl. Fusion (submitted).
[17] K. H. Finken, W. Y. Baek, K. H. Dippel, J. A. Boedo, D. S. Gray, and G. Mank, J. Nucl. Mater. **1**, 220 (1992).
[18] R. P. Doerner *et al.*, Nucl. Fusion **3**, 975 (1994).
[19] J. Cornellis, R. Sporken, G. vanOost, and R. R. Weynants, Nucl. Fusion **3**, 171 (1994).
[20] M. Brix *et al.*, DPG **30**, 177 (1995).
[21] B. Schweer *et al.*, J. Nucl. Mater. **1**, 174 (1992).
[22] A. Messiaen *et al.*, Phys. Plasmas **4**, 1690 (1997).
[23] P. C. Liewer, J. M. McChesney, S. J. Zweben, and R. W. Gould, Phys. Fluids **2**, 309 (1986).
[24] E. J. Powers, Nucl. Fusion **1**, 749 (1974).